Crucial Interplay of Orbital and Cation-Anion Interactions in the Solid State: Distortions of NiO_6 Octahedra in $BaNiLn_2O_5$ Oxides

Jeremy K. Burdett* and John F. Mitchell

Contribution from the Department of Chemistry, James Franck Upton, New Science and Technology Center for Superconductivity, The University of Chicago, Chicago, Illinois 60637. *Received January 19, 1990*

Abstract: The diverse structural features of the three families of oxides belonging to the stoichiometry $BaMLn_2O_5$ (M = Co, Ni, Cu, Zn, Pd, Pt; Ln = Nd, Sm, Eu, Gd, Dy, Ho, Er, Tm, Yb, Lu, or Y) are described. One of these families, typified by the $BaNiGd_2O_5$ structure, possesses a one-dimensional chain of vertex-sharing NiO_6 octahedra running parallel to the crystallographic *a* axis but exhibits a distorted octahedral coordination about Ni^{II}. The Ni-O contacts to the two oxygen ligands along the axis are considerably shorter than those to the four remaining oxygen ligands in the equatorial plane perpendicular to *a* (axial = 1.8936 (2) Å; equatorial = 2.197 (6) Å), a very unusual result. In addition, the equatorial oxygen ligands are distorted away from the right angles of an ideal octahedron to 79.6 (2)°, yielding a D_{2h} local geometry about Ni. These observations are understandable using a model which combines results from molecular orbital theory, tight-binding band structure calculations, and empirical atom-atom potential arguments.

Introduction

The recent explosion of interest in the structure and properties of the high-temperature oxide superconductors extraordinarily kindled oxide chemists' desire to synthesize and characterize an increasingly wide range of interesting materials based on mixed oxides of rare-earth elements and transition metals. These oxides themselves often do not afford high-temperature superconductors but nevertheless can present new structural chemistry of oxide phases and even new structure types. Indeed, a number of such phases have been isolated in conjunction with their superconducting counterparts, unambiguously characterized by X-ray diffraction, and published in the solid-state literature with little notice, undoubtedly because they are largely overshadowed by their superconducting relatives. They are of interest to us not only from a structural point of view but also since they are *not* superconductors. Perhaps too an analysis of their electronic structure will allow access to the question of superconductivity in systems both structurally and stoichiometrically related. In this paper, we will examine one particular series of systems and provide a model combining orbital and empirical atom-atom potential arguments to explain some highly unusual structural features in one of these systems, the $BaMLn_2O_5$ structure family.

The Structures

Transition-metal oxide structures often present us with a fascinating variety of structural building blocks, particularly concerning the coordination environment of the constituent transition metal. The class of compounds belonging to the stoichiometry $BaMLn_2O_5$ (M = Co, Ni, Cu, Zn, Pd, Pt; Ln = Nd, Sm, Eu, Gd, Dy, Ho, Er, Tm, Yb, Lu, or Y) illustrates this point particularly well. Phases of this stoichiometry have been synthesized and characterized by diffraction techniques since the early 1980s by several groups but predominantly by Müller-Buschbaum,[1-10] Raveau and Michel,[11-13] and more recently by Amador et al.[14,15] These groups have found three structure types for this stoichiometry, characterized by three different coordination polyhedra about the transition-metal dication, as pictured in Figure 1. In the $BaCuSm_2O_5$ structure type,[12] copper is 5-fold coordinated by oxygen to form isolated, slightly distorted square pyramids, which are linked through monocapped trigonal prisms of LnO_7. Examples of this structure type are common for copper and can be found also with Co,[1] Ni,[5] or Zn[13] as the transition metal and a variety of trivalent lanthanide cations or yttrium. Importantly, the compound $BaCuY_2O_5$ (the so-called "green phase") can be isolated during the synthesis of the prototypic 1-2-3 superconductor, $YBa_2Cu_3O_{7-x}$.[16,17] For the $BaPtNd_2O_5$ structural family, Pt is found in an isolated square-planar coordination of oxygen atoms. This structure type is far less common than the $BaCuSm_2O_5$ family, possessing only six examples that we are aware of, with Pt,[4,6] Pd,[11] or Cu[18] as the transition metal. Such a transition-metal geometry is the rule for Pd^{II} and Pt^{II} and very common for Cu^{II}. Even in the extended solid the local geometry will be driven by these strong local effects. Finally, in the $BaNiNd_2O_5$ structure type, the transition metal is octahedrally coordinated by oxygen, forming one-dimensional chains of vertex-sharing octahedra propagating parallel to the crystallographic *a* axis. Like $BaCuSm_2O_5$, this is a fairly common structure type, possessing 14 fully characterized members with a wide variety of lanthanide cations but only with Co^{1-3} or $Ni^{5,7,10,14}$ as the transition metal.

(1) Mevs, H.; Müller-Buschbaum, H. *Z. Anorg. Allg. Chem.* **1989**, *574*, 172.
(2) Rühl, H.; Müller-Buschbaum, H. *J. Less Common Metals* **1989**, *152*, 139.
(3) Mevs, H.; Müller-Buschbaum, H. *Z. Anorg. Allg. Chem.* **1989**, *573*, 128.
(4) Müller-Buschbaum, H.; Lang, C. *J. Less Common Metals* **1988**, *142*, L1.
(5) Müller-Buschbaum, H.; Rüter, I. *Z. Anorg. Allg. Chem.* **1989**, *572*, 181.
(6) Schiffler, S.; Müller-Buschbaum, H. *Z. Anorg. Allg. Chem.* **1985**, *523*, 63.
(7) Schiffler, S.; Müller-Buschbaum, H. *Z. Anorg. Allg. Chem.* **1986**, *532*, 10.
(8) Schiffler, S.; Müller-Buschbaum, H. *Z. Anorg. Allg. Chem.* **1986**, *540/541*, 243.
(9) Schiffler, S.; Müller-Buschbaum, H. *Monatsch. Chem.* **1986**, *117*, 465.
(10) Schiffler, S.; Müller-Buschbaum, H. *Monatsch. Chem.* **1987**, *118*, 741.
(11) Laligant, Y.; Fërey, G.; Hervieu, M.; Raveau, B. *Eur. J. Solid State Inorg. Chem.* **1988**, *25*, 111.
(12) Michel, C.; Raveau, B. *J. Solid State Chem.* **1982**, *43*, 73.
(13) Michel, C.; Raveau, B. *J. Solid State Chem.* **1983**, *49*, 150.
(14) Amador, J.; Gutiérrez Puebla, E.; Monge, M. A.; Rasines, I.; Campa, J. A.; Gomez de Salazar, J. M.; Ruiz Valero, C. *Solid State Ionics* **1989**, *32/33*, 123.
(15) Amador, J.; Gutiérrez-Puebla, E.; Monge, M. A.; Rasines, I. *Phys. Rev. B.* Submitted for publication.
(16) Sun, J. Z.; Webb, D. J.; Naito, N.; Char, K.; Hahn, M. R.; Hsu, J. W. P.; Kent, A. D.; Mitzi, D. B.; Oh, B.; Beasley, M. R.; Beballe, T. H.; Hammond, R. H.; Kapitulnik, A. *Phys. Rev. Lett.* **1987**, *58*, 1574.
(17) Hazen, R. M.; Finger, L. W.; Angel, R. J.; Prewitt, C. T.; Ross, N. L.; Mao, H. K.; Hadidiacos, C. G.; Hor, P. H.; Meng, R. L.; Chu, C. W. *Phys. Rev. B* **1987**, *35*, 7238.
(18) Michel, C.; Er-Rakho, L.; Raveau, B. *Rev. Chim. Miner.* **1984**, *21*, 85.

0002-7863/90/1512-6571$02.50/0

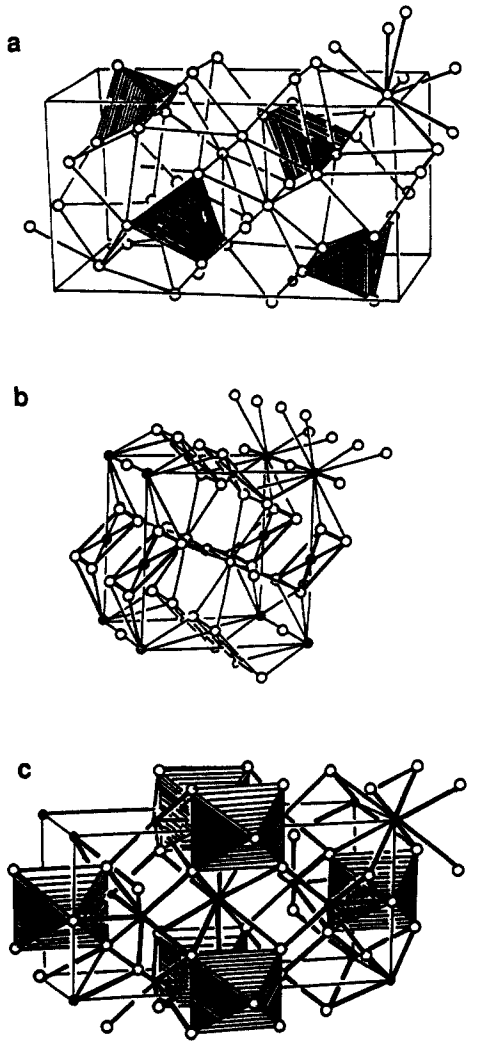

Figure 1. Ball and stick drawings of the three structural families with stoichiometry $BaML_{n_2}O_5$ emphasizing the transition-metal polyhedra: (a) $BaCuSm_2O_5$ structure type (Sm^{3+} cations not shown for clarity) with square pyramids, (b) $BaPtNd_2O_5$ structure type with square planes, (c) $BaNiNd_2O_5$ structure type with vertex-sharing octahedral chains.

Of these structure types, the $BaNiNd_2O_5$ family, with its open framework of octahedral chains, presents perhaps the most fascinating structural features, distinguished by two simple yet unusual distortions away from an ideal octahedral coordination about Ni^{II}. Although not the first known example of this structural type, we focus our discussion on the $BaNiGd_2O_5$ member, as its unusual structure has been recently refined[14] to a precision not obtained in earlier investigations; all metrical parameters refer to this determination. The most striking and unusual feature of the structure concerns the bond lengths between Ni and its six surrounding oxygen ligands. The symmetry of the crystal (space group *Immm*, with Ni in a site of D_{2h} symmetry) requires that all four Ni–O bonds in the equatorial plane perpendicular to [100] be of equal length, in this case 2.197 (6) Å. Additionally, both axial Ni–O bonds (parallel to [100]) must have the same length, here observed as 1.8936 (2) Å. In considering these metrical parameters, we should keep in mind that rocksalt NiO with an ideal octahedral environment about Ni has a Ni–O bond distance of 2.08 Å. We must be somewhat careful here, as NiO is generally considered to have a localized, high-spin configuration.[19] In contrast, we expect $BaNiGd_2O_5$ to adopt a localized, low-spin configuration (vide infra), calling into question comparison of bond lengths between these two systems. However, with no known examples of low-spin Ni^{II} in an octahedral environment, we have chosen NiO as a reasonable model for an undistorted octahedral nickel oxide. Thus, we may consider the Ni coordination in $BaNiGd_2O_5$ as a "two-short + four-long" (2S + 4L) distortion of an octahedron, an unusual distortion in light of the numerous examples of molecular octahedral complexes (particularly of Cu^{II}) distorted in the opposite direction, i.e., 2L + 4S.[20] The second distortion appears as a more subtle angular movement of the equatorial oxygen ligands, which are bent away from an ideal octahedral O–Ni–O angle of 90°, instead appearing with angles of 79.6 (2)° and 100.5 (2)°. **1** illustrates both of these deviations from a regular octahedral environment and identifies the pertinent atoms and the O–Ni–O angle θ which will appear throughout our discussion. Furthermore, we shall refer to the angular distortion of the equatorial ligands as the "D_{2h}" distortion, as this bending motion reduces the local symmetry about Ni from D_{4h} to D_{2h}.

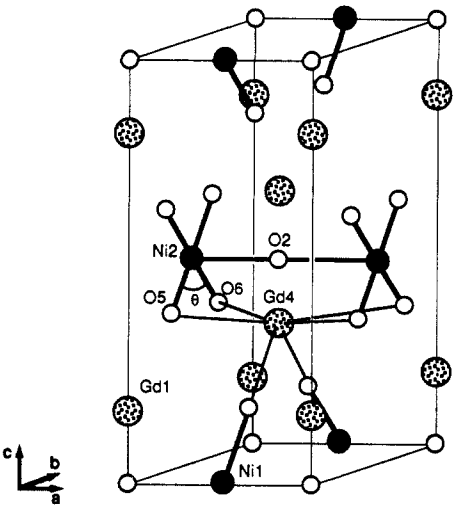

1

In this investigation, we aim to examine the two distortions found in the $BaNiGd_2O_5$ structure under the working assumption that electronic factors peculiar to the vertex-sharing octahedral chain and its surrounding environment provide the driving force for distortion away from an ideal octahedral chain. Because we observe no bond length alternation along the chain, it is clear that the 2S + 4L distortion is not simply an extended Jahn–Teller[21] or Peierls type distortion,[22] so that some other more subtle electronic effect must be at work. As we shall see, the 2S + 4L distortion and the D_{2h} distortion are inextricably linked via the influence of the surrounding lanthanide cations. Indeed, we will find that the 2S + 4L distortion depends strongly upon the D_{2h} geometry about Ni and that the lanthanide cation environment drives the system into the D_{2h} geometry necessary for further distortion along the 2S + 4L coordinate. Our ideas are supported by molecular orbital and band structure calculations using the extended Hückel formalism and "molecular mechanics" calculations which build on an electrostatic potential.

Molecular Models

Examination of discrete molecular analogues which form the building blocks of extended solids has often proved a fruitful approach to understanding the structure of the solid state.[23-26]

(19) West, A. R. *Solid State Chemistry and Its Applications*; Wiley: New York, 1984.

(20) Huheey, J. E. *Inorganic Chemistry*; Harper & Row: New York, 1983; pp 396–406.

(21) Reinen, D.; Frievel, C. In *Structure and Bonding*; Clarke, M. J., et al., Eds.; Springer-Verlag: New York, 1979; pp 1–60.

(22) Peierls, R. E. *Quantum Theory of Solids*; Oxford University Press: Oxford, 1972.

(23) Wheeler, R. A.; Whangbo, M.-H.; Hughbanks, T.; Hoffmann, R.; Burdett, J. K.; Albright, T. A. *J. Am. Chem. Soc.* **1986**, *108*, 2222.

(24) Hoffmann, R. *Solids and Surfaces: A Chemist's View of Bonding in Extended Structures*; VCH Publishers: New York, 1988.

(25) Burdett, J. K.; Kulkarni, G. V.; Levin, K. *Inorg. Chem.* **1987**, *26*, 3650.

(26) Burdett, J. K.; Hughbanks, T. *J. Am. Chem. Soc.* **1984**, *106*, 3101.

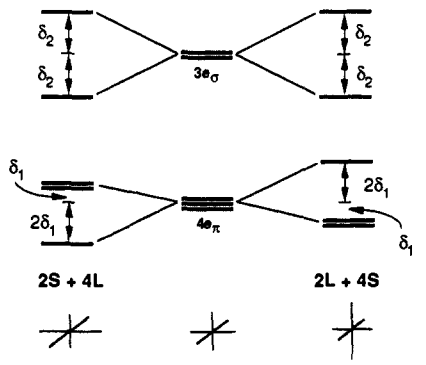

Figure 2. Effect of 2S + 4L and 2L + 4S distortions on the d-orbitals of an octahedral transition-metal complex using the angular overlap model. Only the quadratic terms are assumed significant.

Table I. Angular Overlap Model for Low-Spin Distorted Octahedra

d electron count	low spin (2S + 4L) $-O_h$	low spin (2L + 4S) $-O_h$	high spin (2S + 4L) $-O_h$	high spin (2L + 4S) $-O_h$
d^0	0	0	0	0
d^1	$-2\delta_1$	$-\delta_1$	$-2\delta_1$	$-\delta_1$
d^2	$-4\delta_1$	$-2\delta_1$	$-\delta_1$	$-2\delta_1$
d^3	$-3\delta_1$	$-3\delta_1$	0	0
d^4	$-2\delta_1$	$-4\delta_1$	$-\delta_2$	$-\delta_2$
d^5	$-\delta_1$	$-2\delta_1$	0	0
d^6	0	0	$-2\delta_1$	$-\delta_1$
d^7	$-\delta_2$	$-\delta_2$	$-\delta_1$	$-2\delta_1$
d^8	$-2\delta_2$	$-2\delta_2$	0	0
d^9	$-\delta_2$	$-\delta_2$	$-\delta_2$	$-\delta_2$
d^{10}	0	0	0	0

This is particularly true when such building blocks resemble familiar molecular geometries of transition-metal ions. The three $BaMLn_2O_5$ structure types each fit nicely into this category, possessing a square pyramid, a square plane, or an octahedron of ligands around the transition metal. Of these coordination geometries, the octahedron is perhaps the most familiar to inorganic and coordination chemists. There are countless examples of transition-metal complexes possessing either a true octahedral geometry or a distorted variant.[20] Furthermore, the molecular orbital picture of the electronic structure of such octahedrally coordinated transition-metal complexes is quite familiar and straightforward.[20] For these reasons, our initial approach toward understanding the $BaNiGd_2O_5$ structure will begin with the isolated, discrete octahedron and its distortions along the coordinates observed in the extended solid.

Not only recognizing that the extended Hückel method cannot be relied upon for accurate bond length determinations or absolute total energy estimates but also noting that it will fairly reproduce angular parameters and relative total energies of simple systems, we now look at the possible distortions for a discrete octahedron. Further details of the computations, including all parameters, can be found in the Appendix.

We begin by looking at the orbital effects of the 2S + 4L distortion and its counterpart, the 2L + 4S distortion, for an octahedral ML_6 geometry. Figure 2 shows how the familiar t_{2g} and e_g orbitals of the undistorted metal center split upon moving toward either (2S + 4L or 2L + 4S) D_{4h} distortion. The energy parameters δ_1 and δ_2 will clearly depend strongly on the bond length changes upon distortion. Here we have chosen to keep the d orbital barycenters fixed, implying a true E_g-type distortion in which the axial oxide ligands move twice as far as those in the equatorial plane, an approach we have employed by using the angular overlap model (AOM).[27-29] We have previously demonstrated the utility of this approach in a study of the electronic structure of CrO_2.[30] Table I shows the expected structural preferences as a function of electron count for both high-spin and low-spin complexes along the D_{4h} distortion coordinates. With a d electron count of eight (e.g., high-spin Ni^{II}) $d_{x^2-y^2}$ and d_{z^2} are each occupied with a single electron, and the octahedral complex is Jahn–Teller stable. As exemplified by $Ni(H_2O)_6^{2+}$, this electron configuration prefers a rigorously octahedral geometry. However, for low-spin Ni^{II}, Jahn–Teller unstable, the orbital scheme of Figure 2 predicts a D_{4h} distortion away from an octahedral geometry, though this simple model does not lead to a predicted preference for either a 2S + 4L or a 2L + 4S distortion. We have shown,[28] however, that the 2L + 4S distortion is favored over 2S + 4L due to the low-lying, empty metal s orbital of a_{1g} symmetry, which can mix with the largely d_{z^2} metal–oxygen antibonding orbital and stabilize any electrons occupying it. In the 2L + 4S structure, this d_{z^2} orbital is filled with two electrons, leading to a strong energetic stabilization, but in the 2S + 4L distortion it is empty, and no such electron stabilization can be realized.

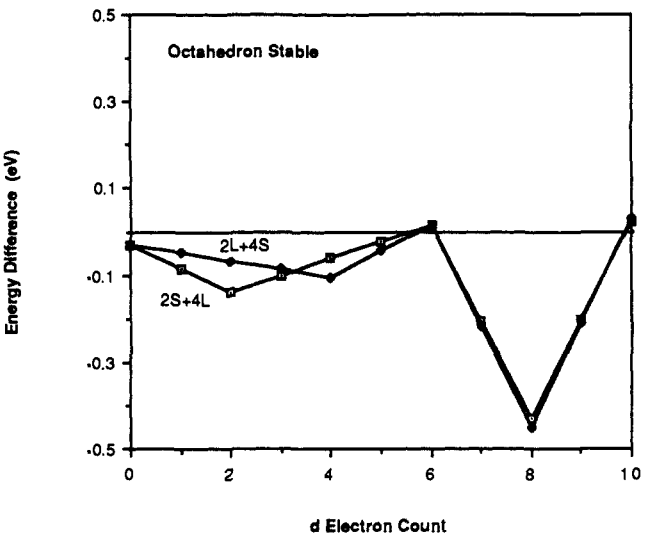

Figure 3. Energy difference curves comparing a regular octahedron to the hypothetical small 2S + 4L and 2L + 4S distortions as a function of electron count.

In the range of bond length changes where we believe the AOM is valid, our extended Hückel calculations on a discrete NiO_6 octahedron undergoing D_{4h} distortions bear out the predictions of Table I quite well. In our initial model calculations, we assume an equilibrium Ni–O distance of 2.08 Å, equal to that in the solid-state structure of NiO, and distort along an E_g coordinate, with $\Delta r_{ax} = 2\Delta r_{eq} = \pm 0.06$ Å, approximately a 3% change in bond length. For such small bond length changes, we believe that the change in orbital energy varies approximately linearly with the change in bond length, i.e., $\Delta E \propto \Delta r$, that the AOM will thus be valid, and that the extended Hückel energies will also remain reliable. Figure 3 shows the low-spin energy preference of the octahedron versus the two D_{4h} distortion modes as a function of electron count. We note that for 2S + 4L the maximum stability appears at electron counts of d^2 and d^8 and that for 2L + 4S they appear at d^4 and again at d^8, precisely as predicted by the simple AOM arguments embodied in Table I. Additionally, we see that for eight d electrons the 2L + 4S structure is slightly favored by 0.023 eV over 2L + 4S, in agreement with our amendment to the AOM, though clearly implying that these structures are quite close in energy.

Still assuming 2.08 Å as a reasonable value for the equilibrium Ni–O distance, we can now look at the larger distortions found experimentally in the solid-state structure, where we find several interesting differences to the small distortion calculations. The observed structure has a short axial Ni–O distance of 1.89 Å and

(27) DeKock, R. L.; Gray, H. B. *Chemical Structure and Bonding*; Benjamin/Cummings: Menlo Park, CA, 1980; pp 391–405.
(28) Burdett, J. K. *Molecular Shapes*; Wiley: New York, 1980; pp 142–195.
(29) Burdett, J. K. *Adv. Inorg. Chem. Radiochem.* **1978**, *21*, 113.
(30) Burdett, J. K.; Miller, G. J.; Richardson, J. W., Jr.; Smith, J. V. *J. Am. Chem. Soc.* **1988**, *110*, 8064.

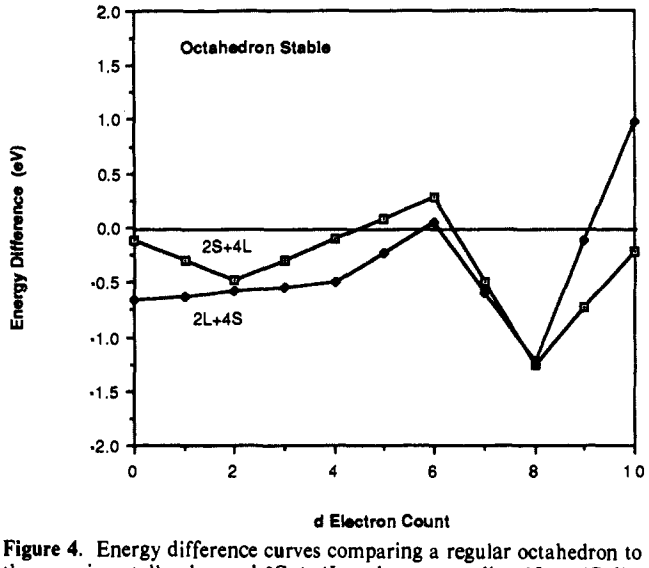

Figure 4. Energy difference curves comparing a regular octahedron to the experimentally observed 2S + 4L and corresponding 2L + 4S distortions as a function of electron count.

a long equatorial distance of 2.20 Å. Thus, our hypothetical 2L + 4S model has a long axial distance of 2.27 Å and a short equatorial distance of 1.96 Å. For these distortions, we point out that $\Delta r_{ax} = 0.19$ Å and $\Delta r_{eq} = 0.12$ Å. As $\Delta r_{ax}/\Delta r_{eq} = 1.58$, this clearly does not conform to an E_g coordinate. The results using this model are shown in Figure 4, again plotting energy difference versus the undistorted octahedron as a function of electron count. In a general sense, this plot resembles that of Figure 3 rather closely, particularly in the region of interest from d^6 to d^8 electrons. A first point of difference is that the d^0 energy preferences are not zero, as predicted by the AOM and borne out in the small D_{4h} distortion regime. As this energy difference reflects interactions among the filled oxygen located orbitals, it represents the nonbonded repulsions or steric effects among the ligands. The d^0 count disfavors the 2S + 4L distortion more than a 2L + 4S distortion, since a 2S + 4L distortion increases eight O–O axial–equatorial repulsions while decreasing only four O–O equatorial–equatorial repulsions and vice versa for the 2L + 4S distortion. Second, at d^{10}, the energy difference is also nonzero, dramatically so for the 2L + 4S distortion. This is a direct consequence of the inclusion of overlap in the extended Hückel method, finds no counterpart in the angular overlap model, and should not be considered significant, particularly since we are interested in the d^8 electron count. Third, we note that at d^8, the energy preference has switched from 2L + 4S to 2S + 4L, favoring the latter by 0.043 eV by our calculations. While this small preference agrees with the observed distortion in the solid state, it contradicts the overriding orbital principles described above. We must consider this result encouraging but suspicious, since we know that the energies determined by our method become unreliable with large bond length changes. However, even for large bond length changes the energy difference is close to zero, and consequently for either small or large D_{4h} distortions the 2S + 4L and 2L + 4S structures are rather close in energy.

We now turn our attention to the other distortion mode observed in the solid state, namely the D_{2h} distortion in the equatorial plane, once again focusing on a molecular NiO_6 complex to understand the orbital interactions upon distortion. Here we compare the D_{2h} distorted octahedron with its symmetrical parent, keeping the bond length fixed at 2.08 Å for each system. We can thus expect the AOM to provide a reliable model, whose results should carry over to the extended Hückel level. The distortion from O_h to D_{2h} removes all orbital degeneracies and allows certain of the e_g and t_{2g} orbitals of the octahedron to mix. We shall see that such symmetry driven orbital interactions play a vital role in the description of the driving force behind the observed distortion.

Figure 5 shows that there are two effects on the d orbitals of the octahedron due to D_{2h} distortion. The first order effect shown in the middle of Figure 5 is due to decreasing overlap between the ligand σ orbitals and the metal d orbitals. First, the decreased overlap with $d_{x^2-y^2}$ stabilizes this formally Ni–O antibonding orbital. However, concurrent with this, the d_{xy} orbital is destabilized by an equal amount (at the AOM level). Due to rigorous orthogonality, the remaining three d orbitals are unaffected in first order. The right-hand side of Figure 5 shows the effect of second-order mixing between d_{xy} and d_{z^2}, allowed by the lower symmetry of D_{2h}. The energies of the d orbitals can be easily computed at the AOM level and are shown for each of the first- and second-order effects, based on the observed angular distortion from 90° to 79.6°. Note that the second-order effect is small ($\beta \approx 0.05 e_\sigma$ for $e_\sigma/e_\pi = 5$) but should become increasingly important as the bond lengths change. We should also note that inclusion of overlap results in the higher lying, more strongly antibonding e_g orbitals becoming more stabilized upon distortion than their t_{2g} counterparts are destabilized, an effect familiar throughout molecular orbital theory.

Since the t_{2g} orbitals are all filled with electrons at d^8, occupation of the e_g set of frontier orbitals will largely determine the energetics of the D_{2h} distortion. Naturally, the occupation of these orbitals will depend on the particular bond length distortion. Under a 2L + 4S distortion, with d_{z^2} occupied and $d_{x^2-y^2}$ empty, electrons in d_{xy} are destabilized in first order with no concomitant stabilization

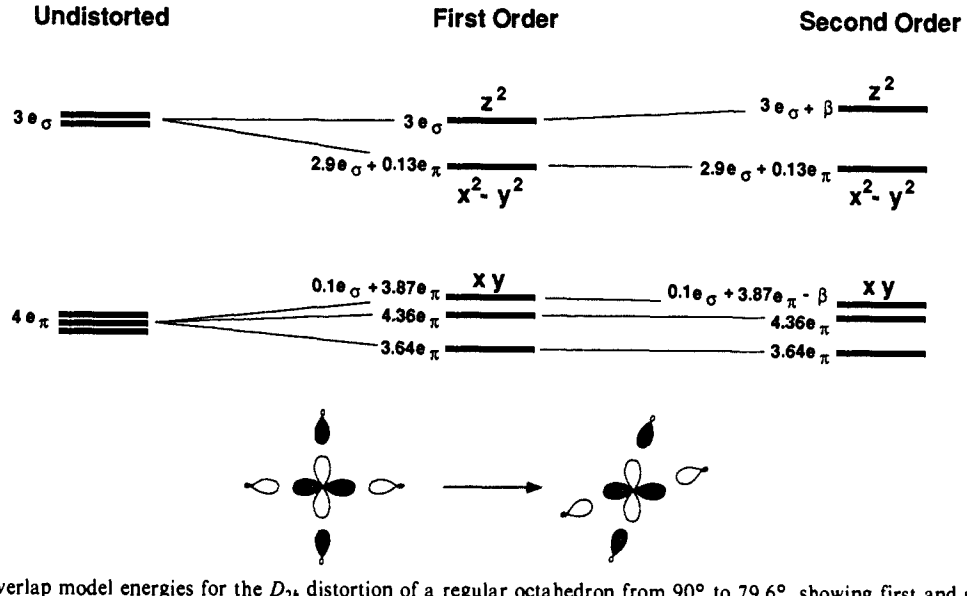

Figure 5. Angular overlap model energies for the D_{2h} distortion of a regular octahedron from 90° to 79.6°, showing first and second order effects. β is the second order energy shift.

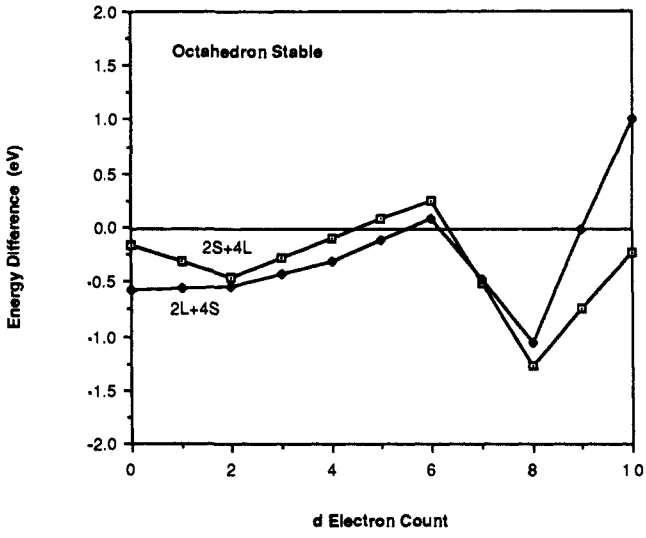

Figure 6. Energy difference curves comparing a regular octahedron to the observed D_{2h} structure with its 2S + 4L and corresponding 2L + 4S distortions as a function of electron count.

of $d_{x^2-y^2}$ electrons. Further, the second-order effect will involve a four-electron, two-orbital interaction, destabilizing the two d_{z^2} electrons. These two factors jointly imply that the D_{2h} distortion should be unfavorable for this occupation. On the other hand, for a 2S + 4L distortion, with $d_{x^2-y^2}$ occupied and d_{z^2} empty, the complex gains stability in first order as the $d_{x^2-y^2}$ orbital is stabilized to a greater extent than d_{xy} is destabilized. This d_{xy} orbital is then further stabilized via a two-electron, two-orbital second-order mixing with d_{z^2}. We note parenthetically that our arguments assume a low-spin occupation of the e_g-derived orbitals, an assumption we will justify later on the basis of the solid-state electronic structure (vide infra). Clearly, these qualitative considerations indicate that the D_{2h} distortion will be favorable for occupation of $d_{x^2-y^2}$ (2S + 4L) but not for occupation of d_{z^2} (2L + 4S).

We are now in a position to consider both the bond length distortion and D_{2h} angular distortion in concert. Our findings are summarized in, i.e., Figure 6, which compares the D_{2h}-distorted structures, with either 2S + 4L or 2L + 4S bond length distortions, to the octahedron; all geometric parameters are those of the solid-state structure. Notice the striking similarity to Figure 4, with the marked difference at d^8, where the D_{2h}-distorted 2S + 4L structure is now favored by a substantial 0.22 eV. We emphasize that the magnitude of this energy difference is subject to all the errors attending the extended Hückel method; however, as evidenced by the arguments above, its direction is a consequence of orbital symmetry arguments alone. That is, the energy preference for 2S + 4L at d^8 indeed results directly from first- and second-order orbital effects accompanying the D_{2h} distortion, establishing that the bond length and angle distortions are closely linked. In fact, we argue that the D_{2h} distortion tips the close energy balance found at the D_{4h} geometry in favor of the observed 2S + 4L distortion over its 2L + 4S counterpart.

One-Dimensional Chain Models

We now move to a more realistic model of the solid-state structure of $BaNiGd_2O_5$, a one-dimensional chain of vertex-sharing octahedra, two of which are found in each unit cell of the three-dimensional structure. The peripheral oxygens of these chains are separated by over 3 Å and are thus essentially noninteracting, justifying our band structure calculations on a single, isolated chain. Although the infinite extent of the chain introduces some complications, we shall find that the picture developed for a discrete molecule carries over largely intact into the solid state and that the orbital effects crucial in discrete octahedra are equally important in the infinite chain.

Figure 7 shows the Ni d band region of the extended Hückel band structure of a chain of ideal octahedra, with Ni–O bond length 2.08 Å. Although the key features of the band structure

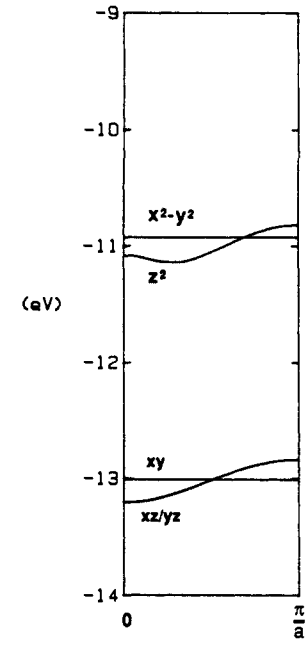

Figure 7. Extended Hückel band structure of a hypothetical vertex-sharing chain of ideal NiO_6 octahedra showing the Ni d-band region.

are quite straightforward, they present a dilemma when trying to establish the ground state of this hypothetical system. As shown in Figure 7, the d_{xy} and $d_{x^2-y^2}$ bands are essentially nondispersive. Such narrow bandwidth arises simply due to the weak δ nature of their overlap from one unit cell to the next along the axis of propagation. The d_{xz} and d_{yz} bands are degenerate throughout the one-dimensional Brillouin zone and being π interactions are significantly more dispersive than d_{xy} or $d_{x^2-y^2}$. Finally, the d_{z^2} band, directed along the chain axis in a σ fashion, has the largest dispersion of all, though still a relatively narrow bandwidth of only 0.3 eV. In the crucial "e_g" region of the band structure, we find the nondispersive $d_{x^2-y^2}$ band cutting the relatively narrow d_{z^2} band. Collectively, these bands hold two electrons at d^8. Narrow bands are often a signature of localized electrons in any number of possible spin states. As our independent electron methods neglect the two-electron terms in the energy, we cannot reliably predict the ground state of this system. However, based on molecular examples of Ni^{II} and on NiO,[19] the two electrons are most likely distributed through both e_g bands in a high-spin fashion, making assessment of the ground state of this hypothetical geometry difficult.

A bond length distortion to 2S + 4L or 2L + 4S clears up this difficulty immediately, justifies our choice of low-spin configurations in the discrete octahedron, and provides a possible rationale for the lack of copper members in the $BaNiGd_2O_5$ structure family. As shown in Figure 8, these distortions separate the bands by a healthy 1.05 eV for 2S + 4L and an even larger 1.62 eV for 2L + 4S. Thus, these hypothetical distorted systems are predicted to be low-spin, diamagnetic insulators, justifying our use of low-spin d^8 Ni^{II} in our molecular models. Note that in the 2S + 4L structure, addition of a ninth d electron begins populating the highly energetic d_{z^2} band, which is strongly antibonding between Ni and the axial O. If this interaction is sufficiently strong, it offers a compelling explanation for the absence of examples of the $BaNiGd_2O_5$ structure type with Cu^{II} as the transition metal.

The effect of a D_{2h} distortion on the octahedral chain with the experimentally determined bond lengths is shown by the band structure in Figure 9, where we see behavior parallel to the discrete octahedron and explicit effects of the infinite extent of the chain. Note that the flat $d_{x^2-y^2}$ band has been stabilized in first order by approximately 0.04 eV and that the d_{z^2} band has been destabilized in second order by roughly 0.01 eV, paralleling the orbital energy shifts found in the discrete octahedron. Once again, we stress the direction rather than the absolute magnitude of such energy shifts. Regarding the second-order orbital mixing in the

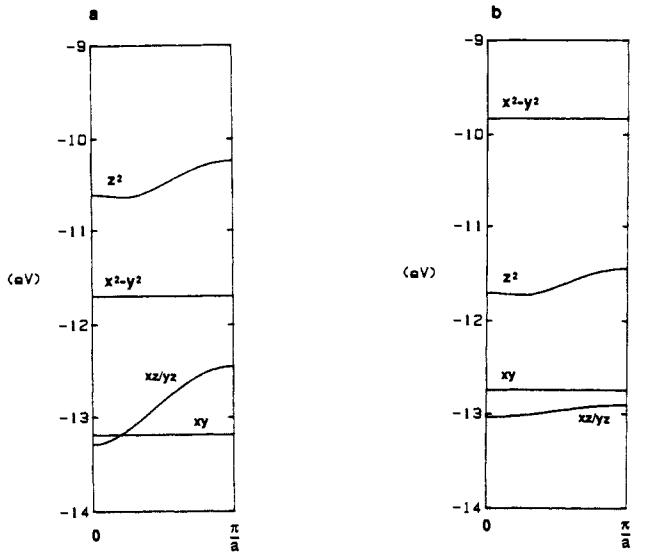

Figure 8. Extended Hückel band structures of the observed 2S + 4L and corresponding 2L + 4S chains in the absence of the D_{2h} distortion showing the Ni d-band region: (a) 2S + 4L and (b) 2L + 4S.

infinite solid, we must take care to recognize that the group of the wavevector for general values of k in the Brillouin zone is isomorphous to C_{2v}, so that the high-lying p_z band also has appropriate symmetry to interact with the d_{z^2} band, stabilizing it. $d_{x^2-y^2}$ finds no such match. However, the d bands lie roughly 5 eV below the metal p bands, so we expect the influence of p band mixing to be small compared to that among the d bands, whose separation is about 2 eV. Indeed, if p band mixing were more important, we would observe a net stabilization of d_{z^2}, in contrast to the observed movement of this band. Interestingly, this band structure has features in common with the two-dimensional CuO_4 sheets of octahedra found in the 2-1-4 high T_c superconductors, with the roles of $d_{x^2-y^2}$ and d_{z^2} interchanged, as illustrated in **2**.

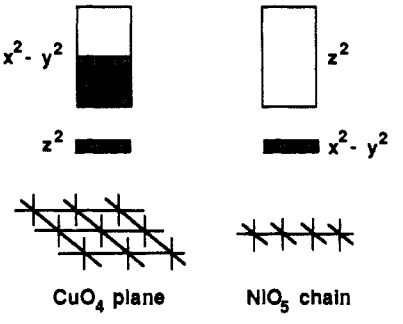

2

Combining the bond length and angle distortions in the one-dimensional chain yields a picture similar to the molecular distortions and one in complete agreement with experiment. Most importantly, we again discover that the D_{2h} distortion is key to favoring the 2S + 4L bond length distortion. The energy difference curves shown in Figure 10 compare the D_{2h} distorted 2S + 4L and 2L + 4S chains to an ideal, undistorted octahedral chain. It bears a striking similarity to Figure 6 from the molecular calculations. Note closely the behavior at d^8. Although less so than the molecular case (0.22 eV), we see that the 2S + 4L structure is favored over 2L + 4S by about 0.06 eV. This is admittedly a small difference, and its value may be subject to errors in the calculation; however, the direction is again completely consistent with our purely orbital and symmetry based arguments. To more clearly show the energetic relationships between distortions, the extended Hückel total energies of several one-dimensional chain systems are shown in Figure 11 on a relative energy scale. At the top center lies the ideal octahedral chain, only slightly more stable by 0.082 eV than its D_{2h} derivative

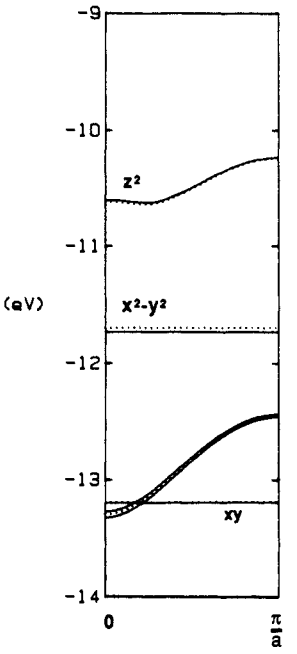

Figure 9. Extended Hückel band structure showing the effect of a D_{2h} distortion on the d-bands of the 2S + 4L structure: solid line, 2S + 4L with D_{2h} distortion; dotted line, 2S + 4L without D_{2h} distortion.

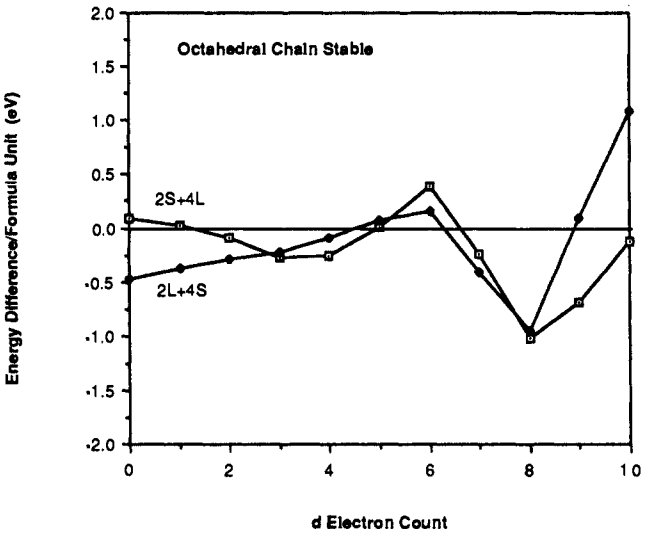

Figure 10. Energy difference curves comparing a regular vertex-sharing octahedral chain to the observed D_{2h} chain with its 2S + 4L and corresponding 2L + 4S distortions as a function of electron count.

structure. At the left and right are the D_{4h} and D_{2h} derivatives of the two bond length distortions, respectively. The diagram clearly shows that the ideal chain is strongly disfavored with respect to either bond length distortion. More importantly, it demonstrates that the 2L + 4S distortion is disfavored by a significant 0.172 eV on bending the equatorial oxygen ligands from D_{4h} to D_{2h}, while the 2S + 4L structure remains essentially isoenergetic (ΔE = 0.003 eV) under the same angular distortion. From the energy diagram and orbital considerations, we thus conclude that given a choice the $D_{4h}/2L + 4S$ structure is the most preferred of these alternatives but that if the chain could be somehow forced into a D_{2h} geometry about Ni, orbital arguments would reverse that preference, favoring the D_{2h}/2S + 4L structure. We now provide persuasive arguments for such a process.

Lanthanide Cation Effects

Thus far, we have followed a conventional approach of considering the $BaNiGd_2O_5$ structure from the so-called "rigid band" method, treating the alkaline-earth and rare-earth cations merely as sources of electrons donated into the energy bands of the

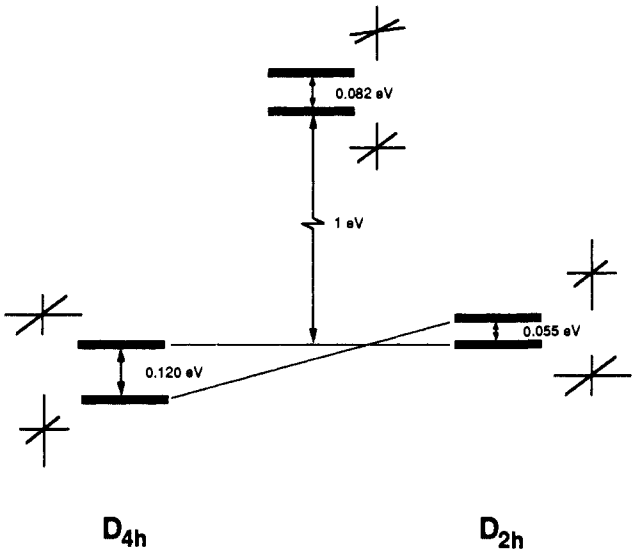

Figure 11. Relative EHT energies of several one-dimensional chains showing the destabilizing effect of the D_{2h} distortion on the 2L + 4S structure.

transition-metal oxide framework. As evidenced by recent work on the high T_c superconductors,[25,31] such an approach frequently meets with success. On the other hand, following ideas championed by Pauling,[32] solid-state chemists typically consider the role of these cations on an equal footing with the transition-metal oxide framework, focusing on the packing of oxygen polyhedra surrounding all cations in the lattice. Indeed, all reports of the $BaNiGd_2O_5$ structure type have been accompanied by such analyses of the coordination polyhedra, emphasizing the chains of NiO_6 octahedra interlocked with monocapped trigonal prisms of GdO_7, as suggested by **1**. Furthermore, the phenomenal deformation of the oxygen polyhedra in the distorted perovskite $GdFeO_3$ testifies to the potent influence of trivalent lanthanide cations on neighboring oxygen atoms.[33] Seeking a mechanism that would drive the equatorial O atoms of the NiO_6 octahedron into a D_{2h} geometry, we now look at the role played by the Gd^{3+} cations proximate to the chains in determining the details of the transition-metal coordination polyhedron.

When considering matters of coordination number and packing, we must always factor in the role of the size of the various cations and anions. However, in the $BaNiNd_2O_5$ structure type, cation size does not seem to correlate with geometric parameters. In fact, both Ni and Co are found with a variety of lanthanides, whose size ranges from the very small Er to the rather large Nd (seven-coordinate, +3 radii = 1.08 Å and 1.19 Å, respectively).[34] Throughout these series of compounds, the equatorial and axial M–O bonds vary by only 0.01–0.03 Å and the O–M–O angle by 1° or less, indicating that cation size, as conventionally defined, has little direct correlation with the observed metrical parameters. Nonetheless, we now show that these cations do play a profound role in the geometric distortions of the structure.

The geometric relationship between the NiO_6 octahedron and its surrounding Gd^{3+} cations suggests that the Gd–O interaction may be crucial to setting the D_{2h} environment at Ni, as corroborated by the dependence of Gd–O metrical parameters on the O(5)–Ni(2)–O(6) angle. Concentrating on the equatorial environment surrounding one of the two equivalent Ni sites (Ni(2), see **1**), we note that the symmetry simplifies our analysis to only two such Gd–O interactions, namely the Gd(1)–O(5) and the Gd(4)–O(5) interactions. From a purely ionic standpoint, the lowest energy structure would bring these two oppositely charged species as close together as possible. If we fix the Gd(1) position,

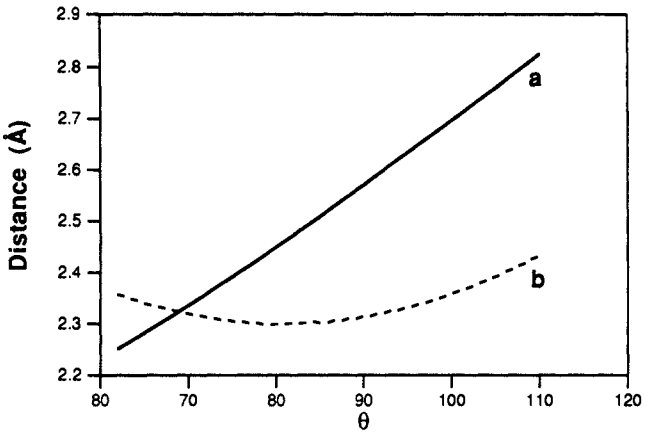

Figure 12. Symmetry-independent Gd–O distances as a function of O–Ni–O angle, θ: curve a, Gd(1)–O(5); curve b, Gd(4)–O(5).

Table II. Atom–Atom Pair Potential Parameters

atom potential	B (eV)	ρ (Å)	C (eV Å^6)
O^{2-}–O^{2-}	1387.7	0.375	63.31
Gd^{3+}–Gd^{3+}	6902.5	0.250	18.44
Gd^{3+}–O^{2-}	3094.2	0.300	34.17

the Ni–O bond length, r, and vary the O–Ni–O angle θ, we sweep out a circle of radius r, which reaches the minimum Gd(1)–O(5) distance when Ni(2), O(5), and Gd(1) are collinear. Curve a of Figure 12 shows a plot of the Gd(1)–O(5) distance dependence on θ. A minimum in the curve occurs at θ = 81.0°, very close indeed to the observed angle in the solid state, 79.6°. Furthermore, the experimental Ni(2)–O(5)–Gd(1) angle is 178.5°, making these three atoms almost, but not quite, collinear. Gd(4) could play a role in determining the O(5)–Ni(2)–O(6) angle, as we may envision it "pulling" O(5) and O(6) together toward the mirror plane at y = 1/2. Curve b of Figure 12 plots the Gd(4)–O(5) distance dependence on θ. As anticipated by inspection, the distance dependence is monotonic, reaching a minimum at the physically unreasonable angle θ = 0°. However, the O(5)–O(6) nonbonded repulsion will overwhelm the Gd–O attraction long before this angle is reached.

Certainly, the striking agreement between the experimentally observed Ni(2)–O(5)–Gd(1) angle and very simple electrostatic arguments tempts us to postulate that Gd(1)–O(5) interactions are the driving force for the D_{2h} distortion. However, the Gd(4)–O(5) type interactions are codirectional with the Gd(1)–O(5) interactions from θ = 90° to 81° and, combined with the O(5)–O(6) repulsions, must not be discounted out of hand. Additionally, a bit of counting shows that there are twice as many Gd(4)–O(5) interactions as Gd(1)–O(5) interactions per formula unit. So, although both suggestive and tempting, simple geometric correlations alone are probably insufficient to establish the relative importance of the various cation–oxygen interactions.

To explore the relative importance of these cation–oxygen terms, we have modeled the pairwise interactions between all species in the structure by using a simple potential which we now briefly describe. We hasten to point out that we find no basis for comparing energies determined via our molecular orbital calculations with those determined by this pairwise potential method. Rather, we employ this latter approach to seek a qualitative understanding of the effects the cation environment has on the chain. In these calculations, the total energy of the structure is assumed to be given by a sum of pairwise potentials, as given by eq 1:[35,36]

$$V = \sum_{i<j} \frac{q_i q_j}{r_{ij}} + B_{ij} \exp\left(\frac{-r_{ij}}{\rho_{ij}}\right) - \frac{C_{ij}}{r_{ij}^6} \qquad (1)$$

(31) Burdett, J. K.; Kulkarni, G. V. *Phys. Rev. B* **1989**, *40*, 8908.
(32) Pauling, L. *The Nature of the Chemical Bond*; Cornell University Press: Ithaca, NY, 1960.
(33) Muller, O.; Roy, R. *The Major Ternary Structural Families*; Springer-Verlag: New York, 1974; pp 187–189.
(34) Shannon, R. D. *Acta Crystallogr.* **1976**, *A32*, 751.
(35) Williams, D. E. In *Crystal Cohesion and Conformational Energies*; Metzger, R. M., Ed.; Springer-Verlag: New York, 1981; pp 3–40.
(36) Whangbo, M.-H.; Evain, M.; Beno, M. A.; Geiser, U.; Williams, J. M. *Inorg. Chem.* **1988**, *27*, 467.

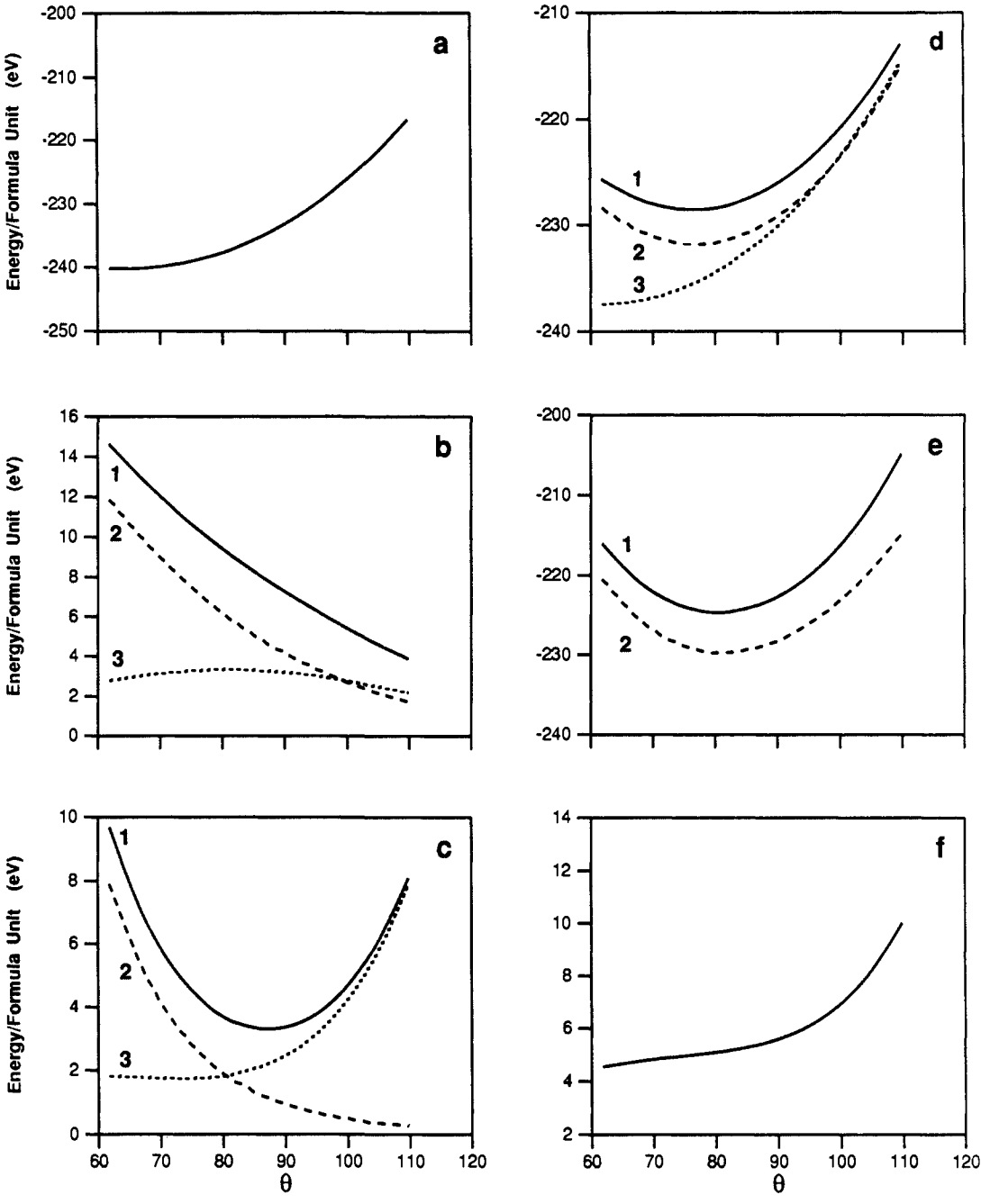

Figure 13. Dependence of atom–atom pair potential energies on O–Ni–O angle, θ: (a) Madelung energy only, (b) Gd–O short-range interactions, (c) O–O short-range interactions, (d) Madelung energy + Gd–O short-range interactions, (e) Madelung energy + Gd–O and O–O short-range interactions, (f) sum of all short-range interactions except Gd(4)–O(5) and O(5)–O(6). See text for details.

The first term in the sum represents the classical Madelung energy of the system and is a long-range pairwise potential requiring a lattice summation for evaluation. The second term is an exponential with decay constant ρ and represents a short-range repulsion term between atomic centers. The final term is also a short-range interaction, associated with an attractive van der Waals force between atoms. Each pairwise potential requires three parameters (B, ρ, and C) which are typically determined by least-squares fitting to the structural parameters of a known phase.[35,36] Table II lists the parameters we used in our calculations.[36] In these calculations, we have included short-range pairwise interactions only between species whose interatomic distances vary with θ, explaining the absence of Ni–O, Ni–Gd, Ni–Ba, Gd–Gd, and Gd–Ba parameters. Indeed, inclusion of these additional short-range terms would only shift the total energy by a factor independent of θ, leaving the value of θ for any energy minimum unaffected. Additionally, we have chosen to ignore the role of Ba–O short-range interactions due to the distance between these cations and the oxygen atoms which move on distortion (Ba–O(2) = 2.92 Å, Ba–O(5) = 2.95 Å).

The six plots in Figure 13 show the effects of the various terms entering into the pairwise total energy calculation and illustrate that a cooperative effect dominated by Gd(4)–O(5) and O(5)–O(6) short-range interactions is indeed responsible for the observed angular parameters. In all of these calculations, each Ni–O distance has been fixed at 2.08 Å so that no 2S + 4L distortion biases the results. Similar calculations using the observed Ni–O bond lengths give precisely the same θ dependence with only a shift in the absolute energy. Figure 13a shows the results of a Madelung calculation on the system, by using the Ewald sum method. Note that the minimum energy lies around θ = 65°, approximately 15° more acute than the observed structure. However, this Madelung calculation explicitly ignores the short-range repulsion terms which can rapidly become important, particularly in light of the O(5)–O(6) nonbonded distance of less than 2.30 Å at this angle! In Figure 13b we show the two com-

Table III. Extended Hückel Atomic Orbital Energies and Exponents

	orbital	H_{ii} (eV)	ζ_1	C_1	ζ_2	C_2
Ni	4s	−9.17	1.825			
	4p	−5.15	1.125			
	3d	−13.49	5.750	0.5683	2.00	0.6292
O	2s	−32.30	2.275			
	2p	−14.80	2.275			

ponents of the Gd–O short-range interactions. Note the remarkable fact that Gd(1)–O(5) short-range interactions (curve 3) are only weakly θ-dependent and that the total Gd–O interaction curve must therefore be almost parallel to the Gd(4)–O(5) curve. (A weak maximum does appear in the Gd(1)–O(5) curve at 81°, suggesting that these interactions may actually disfavor an *exactly* collinear Ni(2)–O(5)–Gd(1) geometry.) The Gd(4)–O(5) short-range interaction curve (curve 2) is strongly θ-dependent, varying over roughly 10 eV in the range shown in Figure 13b. Inspection of the curves alone shows that the total Gd–O curve (curve 1) does indeed almost parallel the Gd(4)–O(5) curve and that up to an additive constant (which cannot affect the position of any minimum in the total energy) the entire Gd–O short-range behavior is determined by this interaction alone. The three curves in Figure 13c show the pertinent O–O short-range interactions. First, notice the strong θ dependence of the O(5)–O(6) interaction (curve 2), particularly below θ = 90°. Accompanying this in the region between approximately 60° and 85° is an essentially θ-independent curve representing the sum of all other O–O interactions (curve 3). These become important only at larger values of θ, well outside our range of interest. Since all O–O interactions other than O(5)–O(6) combine to give a constant energy independent of θ, the total O–O short-range interaction will have a θ dependence essentially parallel to that of O(5)–O(6), at least in the range from 60° to 85°. Indeed, the curve representing the total O–O interaction (curve 1) does parallel the O(5)–O(6) curve in the region of interest, picking up the character of the other interactions only at larger values of θ. The remaining three plots in Figure 13 show the effects of adding in the various short-range terms to the Madelung energy. Note that the curve in Figure 13d representing the Madelung energy plus total Gd–O short-range interaction (curve 1) does parallel that of the curve adding Gd(4)–O(5) alone to the Madelung energy (curve 2). Each curve has a minimum at 78°, close to the observed angle of 79.6°, though slightly more acute. Summing the Madelung energy and the Gd(1)–O(5) interaction (curve 3) fails to produce a minimum in the range shown. Although not presented here, a similar plot for the O–O interactions reveals that in the range from 60° to 85° adding the O(5)–O(6) short-range terms to the Madelung energy parallels the behavior of the Madelung energy plus all O–O short-range interactions. In Figure 13e, we show that summing the Madelung energy, Gd(4)–O(5) interactions, and the O(5)–O(6) interactions yields a curve (curve 2) that is essentially parallel to the curve containing the Madelung energy with all short-range terms added (curve 1). We draw attention to the fact that both of these curves have a minimum at 81°, extremely close to that observed in the X-ray structure. We also mention that the identical calculation performed by using the observed structural parameters (r_{ax} = 1.8936 Å, r_{eq} = 2.197 Å) places this minimum at 80°, even closer to the experimental value.

The final plot in Figure 13 shows the angular dependence of the sum of all short-range terms other than Gd(4)–O(5) and O(5)–O(6). Note particularly that the curve is essentially constant in the region of interest, implying that these remaining terms act substantially as a background on the important Gd(4)–O(5) and O(5)–O(6) terms.

Conclusions

The $BaNiGd_2O_5$ structure presents us with a fascinating combination of energetic factors which work in concert to yield the observed (and highly unusual) structural distortions away from an ideal octahedral chain. As we have shown, the first of these factors arises not from the chain itself but from its surrounding environment of Gd^{3+} cations and in particular the Gd(4)–O(5) type interactions, which "pull" the oxygen ligands O(5) and O(6) in toward $y = 1/2$, finding an energetic minimum at 78°, slightly more acute than the observed angle in the solid state. At this point, the O(5)–O(6) interactions become important, providing a restoring force that opens the angle to approximately 80°, thereby locking in the D_{2h} distortion. We have found that O–O nonbonded repulsions can strongly influence angular parameters for several other transition-metal oxides, notably TiO_2.[37] The second factor develops from orbital electronic effects peculiar to the D_{2h}-distorted octahedral chain. Here, we have shown that the orbitally driven preference for 2L + 4S switches over to 2S + 4L, completing the two types of distortion observed in the structure.

In many cases, the rigid band approach, treating electropositive cations simply as electron sources, is perfectly valid and appropriate. However, our study has shown that where explanations based solely on this approximation fail, investigation of cation geometry and its influence via Madelung energy and the crucial short-range interactions may prove fruitful.

Acknowledgment. This research was supported by the National Science Foundation (DMR 8809854) through the Science and Technology Center for Superconductivity. The authors thank Dr. Thomas Fässler for helpful discussions regarding the role of cations and Dr. Carol Marians for several of the figures. J.F.M. acknowledges the Fannie and John Hertz Foundation for generous support in the form of a fellowship.

Appendix

Both the molecular orbital calculations for the discrete octahedron and the band structure calculations for the solid were performed within the framework of the extended Hückel method[38] with the modified Wolfsberg–Helmholz relation;[39] the parameters used are given in Table III. For the band calculations, 16 special k points were selected in the irreducible wedge of the one-dimensional Brillouin zone by using the method of Monkhorst and Pack.[40] The pair potential calculations were performed by using locally written programs based on the potential developed in ref 35. All parameters for these calculations are given in Table II and are adapted from ref 36.

(37) Burdett, J. K.; Hughbanks, T.; Miller, G. J.; Richardson, J. W., Jr.; Smith, J. V. *J. Am. Chem. Soc.* **1987**, *109*, 3639.
(38) Hoffmann, R. *J. Chem. Phys.* **1963**, *39*, 1397.
(39) Ammeter, J. H.; Bürgi, H.-B.; Thibeault, J.; Hoffmann, R. *J. Am. Chem. Soc.* **1978**, *100*, 3686.
(40) Monkhorst, H. J.; Pack, J. D. *Phys. Rev. B* **1976**, *13*, 5188.